Another mechanism consistent with the experimental data for the reaction of hydridorhodoxime and organic halides involves radical intermediates. Such a possibility is shown by reactions 23–26.

$$HRh(dmgH)_2P(C_6H_5)_3 + RX \rightarrow RH + Rh^{II}(dmgH)_2P(C_6H_5)_3 + X\cdot \quad (23)$$

$$2Rh^{II}(dmgH)_2P(C_6H_5)_3 \rightarrow [Rh^{II}(dmgH)_2P(C_6H_5)_3]_2 \quad (24)$$

$$Rh^{II}(dmgH)_2P(C_6H_5)_3 + X\cdot \rightarrow XRh(dmgH)_2P(C_6H_5)_3 \quad (25)$$

$$HRh(dmgH)_2P(C_6H_5)_3 + X\cdot \rightarrow H^+ + Rh^{II}(dmgH)_2P(C_6H_5)_3 + X^- \quad (26)$$

According to this proposal eq 23 is rate-limiting; the monomeric rhodium(II) complex would have a lifetime similar to at least the $Rh(NH_3)_4^{2+}$ complex.[26] The contrasting features of hydridorhodoxime compared to hydridocobaloxime are that both cobalt complexes, $(Co^I)^-$ and H(Co), are reported[8] to form alkylcobaloximes at comparable rates in protic media (but not in organic solvents; further comments have been given[27]). Hydridorhodoxime, therefore, exhibits more similarities in this regard with $HCo(CN)_5$ which reduces alkyl halides to alkanes[28] and epoxides to alcohols.[29] The reactivity order exhibited by reagents such as $Co(CN)_5^-$ and $(n\text{-}Bu)_3SnH$ which react by free-radical mechanisms with RX is tertiary > secondary > primary. The limited data on hydridorhodoximes, however, are more in keeping with a nucleophilic type mechanism where sterical factors have a larger role than in a free-radical process.

Acknowledgment. This work was supported by the U.S. Department of Energy, Contract W-7405-eng-82, Office of Basic Energy Sciences, Chemical Sciences Division, Budget Code AK-01-03-021.

Registry No. $HRh(dmgH)_2P(C_6H_5)_3$, 21220-16-6; $Rh(dmgH)_2P(C_6H_5)_3^-$, 73597-10-1; *n*-butyl bromide, 109-65-9; $C_6H_5CH_2Cl$, 100-44-7; $C_6H_5CH_2Br$, 100-39-0; $C_6H_5CH(CH_3)Cl$, 672-65-1; $[Rh(dmgH)_2P(C_6H_5)_3]_2$, 21057-94-3; $ClRh(dmgH)_2P(C_6H_5)_3$, 31249-66-8; $ClRh(dmgBF_2)_2P(C_6H_5)_3$, 73597-11-2.

(26) Lilie, J.; Simic, M. G.; Endicott, J. F. *Inorg. Chem.* **1975**, *14*, 2129.

(27) Pratt, J. M.; Craig, P. J. *Adv. Organomet. Chem.* **1973**, *11*, 331–446; see pp 351–355.
(28) Chock, P. B.; Halpern, J. *J. Am. Chem. Soc.* **1969**, *91*, 582.
(29) Kim, J. Y.; Kwan, T. *Chem. Pharm. Bull.* **1970**, *18*, 1040.

Contribution from the Department of Chemistry, West Virginia University, Morgantown, West Virginia 26506

Electron Paramagnetic Resonance and Structural Studies of Small-Ring Metallacycles. Bonding in a Metallacyclopropene Formed by the Oxidative Addition of an Acetylene to Vanadocene

JEFFREY L. PETERSEN* and LINDA GRIFFITH

Received January 16, 1980

A combination of electron paramagnetic resonance and X-ray diffraction methods has been employed to obtain quantitative information about the structural and bonding characteristics associated with acetylene derivatives of vanadocene, $(\eta^5\text{-}C_5H_5)_2V(C_2R_2)$. The outcome of an X-ray diffraction analysis of the dimethyldicarboxyacetylene adduct has revealed that the symmetrical attachment of the acetylene is accompanied by (1) an appreciable canting of the two cyclopentadienyl rings, (2) an ca. 0.08 Å increase in the multiple carbon–carbon distance, and (3) a displacement of the methylcarboxylate substituents such that the C–C–R bond angles have been reduced from 180° (free acetylene) to 143.5° (average). The metallacyclopropene structure (C_{2v}-*mm*2) of the central VC_2 moiety can be described as an isosceles triangle with two equivalent V–C bonds of 2.09 Å (average) and a multiple carbon–carbon bond distance of 1.276 (3) Å. These structural changes associated with the coordinated acetylene reflect its transformation toward the geometry of a cis olefin. Solution and frozen-glass EPR measurements have provided an opportunity to determine the metal-orbital character of the unpaired electron. From computer simulation of the frozen-glass spectrum of $(\eta^5\text{-}C_5H_5)_2V(C_2(CO_2CH_3)_2)$, the values of the principal components of the **g** and T tensors are $g_x = 2.0130$, $g_y = 1.9815$, $g_z = 2.0020$, $T_x = (-)58.5$ G, $T_y = (-)77.0$ G, and $T_z = (-)2.0$ G. On the basis of the same ligand field model applied to d^1 $(\eta^5\text{-}C_5H_5)_2VL_2$ complexes (with the smallest hyperfine component, T_z, directed normal to the plane which bisects the L–V–L bond angle), the anisotropy in the ^{51}V hyperfine interaction similarly arises from an admixture of $3d_{z^2}$ and $3d_{x^2-y^2}$ character in the HOMO of a_1 symmetry for the acetylene complexes. The larger ratio of mixing coefficients, $a(d_{z^2})^2/b(d_{x^2-y^2})^2$, of $-0.995^2/0.100^2 = 99/1$ compared to that for $(\eta^5\text{-}C_5H_4CH_3)_2VCl_2$ of 20/1 is consistent with the appreciably smaller C–V–C bond angle (35.58 (8)°) and reflects a smaller contribution from the $d_{x^2-y^2}$ AO. A qualitative molecular orbital description, which is consistent with the structural and EPR data, is discussed for $(\eta^5\text{-}C_5H_5)_2V(C_2R_2)$ complexes.

Introduction

The interaction of unsaturated molecules such as olefins and acetylenes with transition metals plays a crucial role in a wide variety of chemical processes including polymerization, isomerization, hydrogenation, hydroformylation, and cyclization.[1,2] Olefin and acetylene derivatives are known for bis(cyclopentadienyl) transition-metal complexes of Ti,[3,4] V,[5,6] and Mo[7] and have been suggested as models for reactive intermediates in several of these reactions. In particular, Tsumara and Hagihara[8] have reported that vanadocene catalytically polymerizes acetylene at 80 °C and 250–300 psi. Under milder conditions, however, acetylene derivatives of vanadocene,

(1) Ittel, S. D.; Ibers, J. A. *Adv. Organomet. Chem.* **1976**, *14*, 33, and references cited therein.
(2) Otsuka, S.; Nakamura, A. *Adv. Organomet. Chem.* **1976**, *14*, 245.
(3) Atwood, J. L.; Hunter, W. E.; Alt, H.; Rausch, M. D. *J. Am. Chem. Soc.* **1976**, *98*, 2454.
(4) Fachinetti, G.; Floriani, C.; Marchetti, F.; Mellini, M. *J. Chem. Soc., Dalton Trans.* **1978**, 1398.
(5) Tsumara, R.; Hagihara, N. *Bull. Chem. Soc. Jpn.* **1965**, *38*, 861.
(6) de Liefde Meijer, H. J.; Jellinek, F. *Inorg. Chim. Acta* **1970**, *4*, 651.
(7) (a) Thomas, J. L. *J. Am. Chem. Soc.* **1973**, *95*, 1838. (b) Thomas, J. L. *Inorg. Chem.* **1978**, *17*, 1507.
(8) Tsumara, R.; Hagihara, N. *Bull. Chem. Soc. Jpn.* **1964**, *37*, 1889.

0020-1669/80/1319-1852$01.00/0

$(\eta^5\text{-}C_5H_5)_2V(C_2R_2)$, have been prepared by several investigators[5,6] and are characterized by relatively low carbon–carbon stretching frequencies (1750–1825 cm^{-1}) and by a reduction in the number of unpaired electrons from 3 in vanadocene to 1 in the adducts.[6] Based primarily upon spectroscopic data, a metallacyclopropene structure has been proposed for these acetylene derivatives. Similar complexes have been reported with either an olefin[9] or a diazene[10] bonded to vanadocene. For quantitative information about the stereochemistry and bonding characteristics of the vanadium–acetylene interaction in these complexes, a systematic investigation has been undertaken using a combination of electron paramagnetic resonance and X-ray diffraction methods. Frozen-glass EPR measurements have provided quantitative information about the metal-orbital character of the unpaired electron from an analysis of the ^{51}V hyperfine interaction and thereby have allowed us to examine the relationship between the spatial distribution of the unpaired electron and the nature of the vanadium–acetylene interaction. Consequently, the results of our structural analysis of the dimethyldicarboxyacetylene derivative, $(\eta^5\text{-}C_5H_5)_2V(C_2(CO_2CH_3)_2)$,[11] and EPR measurements on this and related complexes, as described herein, have furnished fundamental information relevant to our general understanding of the interaction of unsaturated organic molecules with early transition metal systems.

Experimental Section

All manipulations were performed under an atmosphere of Ar or N_2 with flame-dried Schlenk glassware. All solvents (reagent grade) were purified and dried by refluxing with sodium/potassium benzophenone ketyl and saturated with Ar prior to use. Vanadium trichloride was purchased from Alfa Ventron and used without further purification. Sample transfers were carried out in N_2- or Ar-purged glovebags (I^2R Lab Products).

Preparation of Compounds. (a) Vanadocene. Lustrous, dark purple crystals of vanadocene were prepared from literature methods[12] with yields of 30–60%. The compound was purified by sublimation (100–120 °C at 0.1 torr) and identified by its characteristic frozen-glass EPR spectrum.[13]

(b) Adducts of Vanadocene. Acetylene, olefin, and diazene derivatives of vanadocene were prepared by the addition of a small excess of the unsaturated organic substrate to a toluene solution of freshly sublimed vanadocene.[5,6] For example, to a stirred toluene solution containing 1.1 g of $(\eta^5\text{-}C_5H_5)_2V$ (6.0 mmol) was added dropwise 1.0 g (7.0 mmol) of dimethyldicarboxyacetylene. The reaction mixture immediately turned dark green, and after 1 h, the solvent was removed in vacuo. Dark green crystals of $(\eta^5\text{-}C_5H_5)_2V(C_2(CO_2CH_3)_2)$ (1.1 g, 3.4 mmol) suitable for X-ray diffraction analysis were isolated by recrystallization from toluene.

Other adducts were prepared in a similar manner from perfluoro-2-butyne, mono- and diphenylacetylene, azobenzene, and octafluoro-2-butene and were identified by their solution EPR spectrum.

Electron Paramagnetic Resonance Measurements. The solution and frozen-glass EPR spectra were recorded on a Varian E-3 spectrometer equipped with a Hewlett-Packard 5340A frequency counter. DPPH was used as the magnetic field marker, and $(\eta^5\text{-}C_5H_4CH_3)_2VCl_2$ was used to calibrate the magnetic field dial of the spectrometer.

Because of the air-sensitive nature of vanadocene and its derivatives, a specially designed quartz EPR tube equipped with a side arm for attachment to a double-manifold vacuum line was used to protect the samples. The solution samples were syringed into the EPR tube under a N_2 or Ar flush and then degassed by freeze–thaw–pump methods. The frozen-glass samples were obtained by the submerging of the tip of the sample tube into a liquid-nitrogen-filled quartz Dewar (Kontes Glass Co.) designed to fit into the microwave cavity of the spectrometer. The field set controls were manually adjusted to determine the magnetic field strength corresponding to specific positions within either the solution or the frozen-glass spectra.

Collection of X-ray Diffraction Data for $(\eta^5\text{-}C_5H_5)_2V(C_2(CO_2CH_3)_2)$. A parallelepiped-shaped crystal with dimensions of 0.25 × 0.35 × 0.45 mm was mounted on the end of a thin-glass fiber with the b axis nearly parallel to the spindle axis of the goniometer. The sample was protected from air and moisture by a thin coating of quick-drying shellac. Preliminary oscillation and Weissenberg photographs taken with Cu Kα radiation indicated the Laue symmetry to be monoclinic C_{2h}-$2/m$. The systematic absences for $\{hkl\}$ of $h + k = 2n + 1$ and $\{h0l\}$ of $l = 2n + 1$ are compatible with two possible space groups, $C2/c$ (C_{2h}^6, no. 15) and Cc (C_s^4, no. 9). The sample was transferred to a Picker goniostat under computer control by a Krisel Control diffractometer automation system. The angular coordinates $(\omega, \chi, 2\theta)$ for 20 diffraction peaks with a 2θ range of $29° < 2\theta < 35°$ were optimized by the automatic-centering routine and least squares refined to yield unit cell parameters with a = 25.083 (5) Å, b = 7.944 (3) Å, c = 15.984 (4) Å, β = 112.23 (2)°, V = 2948 (1) Å^3, Z = 8, and ρ_{calcd} = 1.456 g/cm^3.

Intensity data $(hkl, \bar{h}kl)$ were measured with Zr-filtered Mo Kα X-ray radiation within a detector range of $3° \le 2\theta \le 50°$ with the takeoff angle set at 2.0°. The θ–2θ scan mode was employed with a fixed scan rate of 2°/min and variable scan widths, w, calculated from the expression $1.0 + 0.7 \tan\theta$. Ten-second background counts were measured at the extremes of each scan. The pulse-height analyzer of the scintillation detector was adjusted to accept 90% of the diffraction peak. The intensities of three standard reflections were measured after every 120 min of sample exposure, and their combined value did not exceed a 3% variation during the data collection period. The integrated intensity, I, and its standard deviation, $\sigma_c(I)$, for each peak were calculated from the respective expressions $I = w(S/t_s - B/t_b)$ and $[\sigma_c(I)]^2 = w^2(S/t_s^2 + B/t_b^2)$. In these equations S represents the total scan count measured in time t_s and B is the combined background count in time t_b. The intensity data were corrected for background and Lorentz–polarization effects. The standard deviation of the square of each structure factor, $F_o^2 = I/Lp$, was calculated from $[\sigma(F_o^2)]^2 = [\sigma_c(F_o^2)]^2 + (0.03F_o^2)^2$ where $[\sigma_c(F_o^2)]^2$ is determined from counting statistics and 0.03 is an empirical factor which accounts for the variation of the integrated intensities of the reference reflections. Duplicate reflections were averaged to provide 2611 unique reflections with $F_o^2 \ge 0$. All data were used initially in the structural analysis. However, near the end of the refinement the two strongest reflections (402 and 312) were removed because of counter saturation effects.

Analysis of the EPR Spectra. The solution EPR spectra for all of the vanadocene derivatives which were examined contain eight well-resolved lines characteristic of the hyperfine coupling of the unpaired electron with the nuclear magnetic moment of the ^{51}V nucleus (99.8% abundance, $I = {}^7/_2$). The corresponding isotropic parameters for $(\eta^5\text{-}C_5H_5)_2V(C_2(CO_2CH_3)_2)$ of (−)43.4 G and g_{iso} = 1.9968 were determined from a modified form of the Breit–Rabi equation.[14] Similar spectra were obtained for a variety of other acetylenes, azobenzene, and octafluoro-2-butene.[15] The small range of 43–46 G for the isotropic coupling constants suggests that A_{iso} is relatively invariant to substituents on the acetylene and that these three types of unsaturated organic substrates bond to vanadocene in a similar manner.

The corresponding frozen-glass EPR spectra such as depicted in Figure 1 for $(\eta^5\text{-}C_5H_5)_2V(C_2(CO_2CH_3)_2)$ contain a complex pattern of overlapping hyperfine lines. To estimate the magnitude of the principal components of the electron Zeeman, **g**, and hyperfine, **T**, tensors, computer simulation of the observed spectra was performed by varying the values of the magnetic parameters included in the spin Hamiltonian until a reasonable fit was obtained for an assumed line shape and isotropic line width. The essential features of the frozen-glass EPR spectra for the dimethyldicarboxyacetylene (g_x = 2.0013,[16] g_y = 1.9815, g_z = 2.0020, T_x = −58.5 G, T_y = −77.0 G, T_z

(9) Fachinetti, G.; Floriani, C.; Chiesa-Villa, A.; Guastini, C. *Inorg. Chem.* **1979**, *18*, 2282.
(10) Fachinetti, G.; Fochi, G.; Floriani, C. *J. Organomet. Chem.* **1973**, *57*, C51.
(11) At the time of submission, an X-ray diffraction study was reported for the dimethyldicarboxyacetylene derivative by Floriani and co-workers.[9] The two independently determined structures agree within experimental error.
(12) Eisch, J. J.; King, R. B. "Organometallic Synthesis"; Academic Press: New York, 1965; Vol. 1, p 64.
(13) Prins, R.; Biloen, B.; van Voorst, J. *J. Chem. Phys.* **1967**, *46*, 1216.
(14) Weil, J. A. *J. Magn. Reson.* **1971**, *4*, 394.
(15) The isotropic hyperfine coupling constants for the perfluoro-2-butyne, phenylacetylene, diphenylacetylene, azobenzene, and octafluoro-2-butene derivatives are (−)44.6 G, (−)44.8 G, (−)43.1 G, (−)45.2 G, and (−)45.0 G, respectively.

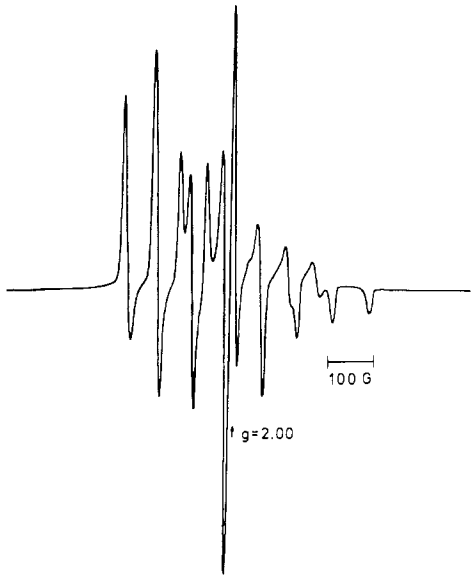

Figure 1. Frozen-glass EPR spectrum of $(\eta^5\text{-}C_5H_5)_2V(C_2(CO_2CH_3)_2)$.

= −2.0 G), hexafluoro-2-butyne (g_x = 2.0090, g_y = 1.9810, g_z = 2.0020, T_x = −62.5 G, T_y = −77.5 G, T_z = −2.0 G), and azobenzene (g_x = 2.0060, g_y = 1.9815, g_z = 2.0020, T_x = −65.5 G, T_y = −77.5 G, T_z = −2.0 G) adducts were easily simulated from a second-order expression[17-19] derived from perturbation theory for a $S = {}^1/_2$ system with the principal axes of the magnetic tensors being coincident. The values of the principal components of the **g** and **T** tensors reflect the nonaxial environment about the vanadium atom. In contrast to the isotropic parameters which remain relatively constant, the corresponding anisotropic parameters (especially g_x and T_x) appear to be sensitive to changes in the acetylene substituents as well as the bound substrate.

Structural Analysis of $(\eta^5\text{-}C_5H_5)_2V(C_2(CO_2CH_3)_2)$. The approximate fractional coordinates for 15 of the 21 nonhydrogen atoms were provided by the first E map calculated with the use of the phase assignments for the set with the highest figure of merit from MULTAN 78.[20] A subsequent Fourier synthesis provided the coordinates of the remaining six nonhydrogen atoms. Initial coordinates for the cyclopentadienyl ring hydrogen atoms were calculated with MIRAGE.[21] The methyl hydrogen atoms were located by difference Fourier methods. Full-matrix least-squares refinements on F_o^2 with anisotropic temperature factors for the 21 nonhydrogen atoms and isotropic temperature factors for the 16 hydrogen atoms converged with $R(F_o)$ = 0.0366, $R(F_o^2)$ = 0.0445, and $R_w(F_o^2)$ = 0.0813 and the standard deviation of an observation of unit weight σ_1 equal to 1.83 for the 2609 reflections.[22-26] The maximum parameter shift to error ratio was 0.10 during the last refinement cycle. A final difference Fourier synthesis was virtually featureless with no residual electron density greater than 0.25 e/Å^3 and thereby verified the completeness and correctness of the structural analysis and refinement.

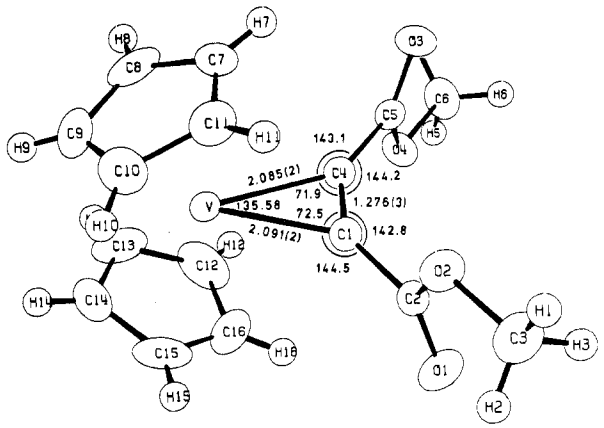

Figure 2. Molecular configuration of $(\eta^5\text{-}C_5H_5)_2V(C_2(CO_2CH_3)_2)$ with atom labeling scheme. Bond distances and angles associated with the central metallacyclopropene moiety are given. Atom H4 is hidden behind O3. The thermal ellipsoids were scaled to enclose 50% probability.

Positional and anisotropic thermal parameters from the output of the last least-squares cycle are provided in Table I. Interatomic distances and bond angles with their corresponding estimated standard deviations calculated from the variance–covariance matrix are given in Table II. These structural parameters are comparable to those reported recently by Floriani and co-workers[9] for the same acetylene adduct. Least-squares planes of interest and a table of the calculated and observed structure factors are available as supplementary material.[27]

Discussion of Results

Molecular Configuration of $(\eta^5\text{-}C_5H_5)_2V(C_2(CO_2CH_3)_2)$. The molecular configuration of the dimethyldicarboxyacetylene derivative of vanadocene, $(\eta^5\text{-}C_5H_5)_2V(C_2(CO_2CH_3)_2)$, is illustrated in Figure 2 with the appropriate atom labeling scheme. The overall molecular geometry closely resembles that commonly observed for canted bis(cyclopentadienyl)metal complexes, $(\eta^5\text{-}C_5H_5)_2ML_2$.[29] With the assumption of cylindrical symmetry for the cyclopentadienyl rings, the ligand arrangement about the vanadium atom nearly conforms to C_{2v}-$mm2$ symmetry. The bond distances and angles associated with the vanadium–acetylene interaction indicate that the acetylene molecule is symmetrically attached to the vanadium via two σ-type V–C bonds of 2.09 Å (average) producing a metallacyclopropene structure for the central VC_2 moiety. The 0.08-Å increase of the multiple carbon–carbon distance to 1.276 (3) Å reflects the reduction of its bond order upon acetylene coordination. This effect presumably results from back-donation of electron density from the metal to an empty π^*-antibonding acetylene orbital (vide infra). A similar but asymmetric structure has been reported by Teuben and coworkers for $(\eta^5\text{-}C_5H_5)_2Ti(C_6H_5N\text{-}2,6\text{-}(CH_3)_2C_6H_3)$.[29] The

(16) One unusual feature of the EPR parameters is that the value of the g_x component is greater than the free-electron value of 2.0023 in each case. Normally for d^1 vanadium systems spin–orbit coupling effects reduce all Zeeman components below 2.0 with the largest hyperfine component associated with the smallest g component and vice versa. Since g_x is directed toward the multiple carbon–carbon bond, this variation must be closely related to the nature of the metal–acetylene interaction.
(17) Taylor, P. C.; Baugher, J. F.; Kriz, H. M. *Chem. Rev.* **1975**, *75*, 203.
(18) This expression has been incorporated into a locally modified version of a general EPR computer simulation program, originally written by Taylor and Bray.[19]
(19) (a) Taylor, P. C.; Bray, P. J. Lineshape Program Manual, Physics Department, Brown University, Providence, RI, 1968 (unpublished). (b) Taylor, P. C.; Bray, P. J. *J. Magn. Reson.* **1970**, *2*, 305.
(20) Declerq, J. P.; Germain, D.; Main, P.; Woolfson, M. M. *Acta Crystallogr., Sect. A* **1973**, *29*, 231.
(21) Calabrese, J. C. MIRAGE, Ph.D. Thesis (Appendix II), University of Wisconsin, Madison, WI, 1971.
(22) The least-squares refinements of the X-ray diffraction data were based upon the minimization of $\sum w_i|F_o^2 - S^2F_c^2|$, where the individual weights, w_i, equal $1/[\sigma(F_o^2)]^2$ and S is the scale factor. The discrepancy indices were calculated from the expressions $R(F_o) = [\sum||F_o| - |F_c||/\sum|F_o|]$, $R(F_o^2) = \sum|F_o^2 - F_c^2|/\sum F_o^2$, and $R_w(F_o^2) = [\sum w_i|F_o^2 - F_c^2|^2/\sum w_iF_o^4]^{1/2}$. The final goodness-of-fit parameters, $\sigma_1 = [\sum w_i|F_o^2 - F_c^2|/(n-p)]^{1/2}$, where n is the number of observations and p is the number of parameters (viz., 238), varied. The final data-to-parameter ratio is 11:1.
(23) The scattering factors utilized in all calculations were those of Cromer and Mann[24] for the nonhydrogen atoms and those of Stewart et al.[25] for the hydrogen atoms with corrections included for anomalous dispersion.[25]
(24) Cromer, D. T.; Mann, J. *Acta Crystallogr., Sect. A* **1968**, *24*, 321.
(25) Stewart, R. F.; Davidson, E. R.; Simpson, W. T. *J. Chem. Phys.* **1965**, *42*, 3175.
(26) Cromer, D. T.; Liberman, D. *J. Chem. Phys.* **1970**, *53*, 1891.
(27) The computer programs used to perform the necessary calculations are described in: Petersen, J. L. *J. Organomet. Chem.* **1979**, *155*, 179.
(28) Prout, K.; Cameron, T. S.; Forder, R. A.; Critchley, S. R.; Denton, B.; Rees, G. V. *Acta Crystallogr., Sect. B* **1974**, *30*, 2290 and references cited therein.
(29) van Bolhuis, F.; de Boer, E. J. M.; Teuben, J. H. *J. Organomet. Chem.* **1979**, *170*, 299.

Table I. Positional and Thermal Parameters for $(\eta^5\text{-}C_5H_5)_2V(C_2(CO_2CH_3)_2)$[a,b]

A. Positional Parameters

atom	x	y	z	atom	x	y	z
V	0.374 00 (1)	0.052 57 (4)	0.803 37 (2)	C15	0.451 19 (12)	−0.120 89 (33)	0.830 25 (29)
O1	0.439 97 (7)	0.163 29 (21)	0.609 58 (11)	C16	0.413 64 (20)	−0.156 50 (37)	0.746 33 (24)
O2	0.423 65 (6)	0.406 99 (17)	0.664 64 (11)	H1	0.458 9 (13)	0.598 9 (41)	0.633 1 (21)
O3	0.233 65 (6)	0.222 01 (20)	0.588 00 (10)	H2	0.496 9 (15)	0.435 4 (39)	0.648 2 (22)
O4	0.258 73 (6)	−0.030 17 (17)	0.551 84 (10)	H3	0.447 6 (15)	0.479 8 (38)	0.563 4 (24)
C1	0.377 72 (8)	0.169 75 (23)	0.688 55 (12)	H4	0.171 7 (14)	−0.024 9 (38)	0.510 5 (22)
C2	0.415 76 (8)	0.241 64 (24)	0.649 32 (12)	H5	0.201 2 (12)	−0.175 2 (40)	0.460 7 (19)
C3	0.461 46 (14)	0.487 81 (39)	0.628 16 (23)	H6	0.196 7 (14)	0.029 8 (38)	0.435 1 (23)
C4	0.326 53 (8)	0.115 64 (24)	0.669 01 (12)	H7	0.286 6 (14)	0.296 3 (38)	0.775 8 (21)
C5	0.269 00 (8)	0.112 49 (25)	0.599 61 (13)	H8	0.286 6 (14)	0.072 9 (39)	0.872 8 (22)
C6	0.201 56 (11)	−0.046 45 (36)	0.482 69 (17)	H9	0.382 9 (14)	0.047 1 (39)	0.982 4 (23)
C7	0.317 64 (11)	0.266 98 (32)	0.820 42 (17)	H10	0.448 9 (13)	0.245 4 (39)	0.949 5 (21)
C8	0.316 91 (15)	0.136 90 (38)	0.877 40 (23)	H11	0.386 4 (14)	0.409 2 (42)	0.818 9 (21)
C9	0.373 51 (18)	0.120 97 (41)	0.941 16 (18)	H12	0.336 8 (14)	−0.246 7 (41)	0.712 1 (22)
C10	0.407 67 (13)	0.234 99 (38)	0.920 61 (18)	H13	0.355 3 (14)	−0.253 0 (42)	0.861 7 (23)
C11	0.373 45 (13)	0.326 02 (30)	0.847 39 (18)	H14	0.445 1 (13)	−0.147 9 (40)	0.949 5 (22)
C12	0.364 33 (15)	−0.217 19 (32)	0.752 49 (25)	H15	0.485 1 (14)	−0.061 2 (38)	0.837 8 (21)
C13	0.373 07 (16)	−0.219 63 (32)	0.842 38 (31)	H16	0.413 7 (13)	−0.152 4 (39)	0.691 5 (22)
C14	0.427 22 (15)	−0.160 96 (37)	0.889 15 (18)				

B. Temperature Factors

atom	U_{11}	U_{22}	U_{33}	U_{12}	U_{13}	U_{23}
V	408 (2)	323 (2)	376 (2)	40 (1)	185 (1)	6 (1)
O1	793 (11)	639 (10)	745 (10)	−28 (8)	510 (9)	−79 (8)
O2	594 (9)	440 (8)	719 (10)	−81 (7)	340 (8)	−5 (7)
O3	474 (8)	631 (10)	684 (10)	154 (7)	215 (7)	12 (8)
O4	461 (8)	461 (8)	536 (8)	11 (6)	61 (6)	−3 (7)
C1	431 (10)	386 (10)	390 (9)	0 (8)	152 (7)	6 (8)
C2	403 (10)	443 (11)	347 (9)	10 (8)	117 (8)	21 (8)
C3	744 (18)	647 (16)	945 (20)	−159 (14)	432 (16)	102 (16)
C4	439 (11)	419 (10)	398 (10)	27 (8)	162 (8)	11 (8)
C5	408 (10)	454 (10)	434 (10)	10 (9)	207 (8)	55 (8)
C6	515 (13)	687 (16)	553 (14)	−124 (12)	14 (11)	57 (12)
C7	683 (16)	667 (15)	595 (14)	295 (13)	255 (12)	−56 (12)
C8	1017 (23)	724 (18)	1014 (22)	−12 (16)	794 (21)	−159 (17)
C9	1566 (33)	715 (18)	489 (14)	513 (21)	534 (19)	115 (13)
C10	823 (18)	752 (18)	578 (15)	152 (15)	100 (14)	−256 (14)
C11	931 (19)	401 (12)	708 (16)	48 (12)	402 (14)	−105 (11)
C12	888 (21)	398 (13)	964 (24)	65 (14)	−23 (18)	−213 (14)
C13	1108 (27)	369 (13)	1717 (38)	195 (15)	1078 (29)	317 (17)
C14	983 (23)	642 (16)	596 (15)	426 (16)	198 (15)	88 (13)
C15	550 (15)	520 (15)	1464 (33)	130 (12)	481 (19)	31 (17)
C16	1562 (34)	569 (16)	907 (22)	480 (20)	883 (25)	189 (16)

[a] The estimated standard deviations in parentheses for this and all subsequent tables refer to the least significant figures. [b] The form of the anisotropic temperature factors ($\times 10^4$) is $\exp[-2\pi^2(h^2a^{*2}U_{11} + k^2b^{*2}U_{22} + l^2c^{*2}U_{33} + 2hka^*b^*U_{12} + 2hla^*c^*U_{13} + 2klb^*c^*U_{23})]$. The isotropic temperature factor, given by $\exp[-8\pi^2U(\sin^2\theta)/\lambda^2]$, is 0.101 Å^2 for all H atoms.

iminoacyl ligand bonds to the Ti atom with Ti–C and Ti–N separations of 2.096 (6) and 2.149 (4) Å, respectively. The acute C1–V–C4 bond angle of 35.58 (8)° is substantially smaller than the corresponding L–M–L bond angles in $(\eta^5\text{-}C_5H_5)_2ML_2$ complexes, which range from 76 to 105° depending upon L and the electronic configuration of the metal.[30] In general, as the number of nonbonding electrons on the metal increases from 0 to 1 to 2, the L–M–L bond angle decreases with an accompanying increase in the M–L bond distance. Although insufficient structural data on the corresponding acetylene derivatives is available to make a similar correlation, the stereochemical effect of the metal's electronic configuration upon the C–M–C angle probably is less pronounced in these metallacyclic complexes since this angle is further constrained by the magnitude of the multiple C–C and M–C bond distances. The degree to which substituent effects (either steric and/or electronic) can modify these bonding parameters associated with the vanadacyclopropene structure is currently not known and thereby suggests the need for further structural studies.

Another important structural consideration is the geometrical alterations which accompany the acetylene upon coordination. The methylcarboxylate substituents are displaced such that the C–C–R bond angles are reduced from 180° in a free acetylene molecule to 143.5° (average) in the vanadocene adduct. The nonhydrogen atoms within each of the two methylcarboxylate substituents are coplanar, and their corresponding planes are essentially perpendicular to the central vanadacyclic plane. Carbon atoms C2 and C5 are displaced 0.144 (2) Å below and 0.080 (3) Å above the VC_2 plane, respectively, with a C5–C4–C1–C2 torsional angle of 14.8 (5)°. These observed structural changes which occur upon coordination clearly reflect the acetylene's transformation toward the geometry of a cis olefin.

Qualitative Bonding Description for Acetylene Derivatives of Vanadocene. The earliest models which were developed to describe the interaction of unsaturated molecules, primarily olefins, with transition metals were proposed by Dewar[31] and Chatt and Duncanson in 1953.[32] The essential aspect of either approach is that the two carbon p_z orbitals of the olefin provide

(30) Schultz, A.; Stearley, K. L.; Williams, J. M.; Mink, R.; Stucky, G. D. *J. Am. Chem. Soc.* **1977**, *16*, 3303 and references cited therein.

(31) Dewar, M. J. S. *Bull. Soc. Chim. Fr.* **1951**, *18*, C71.

(32) Chatt, J.; Duncanson, L. A. *J. Chem. Soc.* **1953**, 2939.

Table II. Interatomic Distances (Å) and Bond Angles (Deg) for $(\eta^5\text{-}C_5H_5)_2V(C_2(CO_2CH_3)_2)$[a]

(A) Interatomic Distances

V-C1	2.091 (2)	V-C4	2.085 (2)
V-C7	2.295 (3)	V-C12	2.272 (3)
V-C8	2.276 (4)	V-C13	2.253 (3)
V-C9	2.273 (3)	V-C14	2.270 (3)
V-C10	2.264 (3)	V-C15	2.281 (3)
V-C11	2.285 (3)	V-C16	2.294 (4)
C1-C2	1.443 (3)	C4-C5	1.450 (2)
C2-O1	1.205 (3)	C5-O3	1.205 (3)
C2-O2	1.337 (2)	C5-O4	1.336 (2)
O2-C3	1.439 (4)	O4-C6	1.448 (3)
C1-C4	1.276 (3)	C12-C13	1.369 (6)
C7-C8	1.382 (4)	C13-C14	1.361 (5)
C8-C9	1.406 (5)	C14-C15	1.333 (6)
C9-C10	1.370 (5)	C15-C16	1.346 (5)
C10-C11	1.367 (4)	C16-C12	1.365 (6)
C11-C8	1.382 (4)	C6-H4	1.02 (4)
C3-H1	0.89 (3)	C6-H5	1.08 (3)
C3-H2	0.92 (3)	C6-H6	0.94 (3)
C3-H3	0.96 (4)	C12-H12	0.78 (3)
C7-H7	0.87 (3)	C13-H13	0.68 (4)
C8-H8	0.89 (4)	C14-H14	0.90 (3)
C9-H9	0.85 (3)	C15-H15	0.94 (3)
C10-H10	0.96 (3)	C16-H16	0.88 (4)
C11-H11	0.93 (4)		

(B) Bond Angles

C1-V-C4	35.58 (8)		
V-C1-C4	71.9 (1)	V-C4-C1	72.5 (1)
V-C1-C2	144.5 (1)	V-C4-C5	143.1 (2)
C4-C1-C2	142.8 (2)	C1-C4-C5	144.2 (2)
C1-C2-O1	124.9 (2)	C4-C5-O3	124.5 (2)
C1-C2-O2	112.7 (2)	C4-C5-O4	111.9 (2)
O1-C2-O2	122.3 (2)	O3-C5-O4	123.5 (2)
C2-O2-C3	116.0 (2)	C5-O4-C6	115.7 (2)
C11-C7-C8	108.2 (2)	C16-C12-C13	106.9 (3)
C7-C8-C9	106.5 (3)	C12-C13-C14	107.6 (4)
C8-C9-C10	108.6 (3)	C13-C14-C15	108.5 (3)
C9-C10-C11	107.9 (3)	C14-C15-C16	108.7 (3)
C10-C11-C7	108.7 (3)	C15-C16-C12	108.3 (4)
H1-C3-O2	109 (3)	H4-C6-O4	109 (2)
H2-C3-O2	110 (2)	H5-C6-O4	102 (2)
H3-C3-O2	112 (2)	H6-C6-O4	110 (2)
H1-C3-H2	121 (3)	H4-C6-H5	113 (3)
H1-C3-H3	99 (3)	H4-C6-H6	111 (3)
H2-C3-H3	105 (3)	H5-C6-H6	111 (3)
H7-C7-C11	131 (2)	H12-C12-C16	126 (3)
H7-C7-C8	121 (2)	H12-C12-C13	127 (3)
H8-C8-C7	126 (2)	H13-C13-C12	127 (3)
H8-C8-C9	127 (2)	H13-C13-C14	125 (3)
H9-C9-C8	122 (2)	H14-C14-C13	128 (2)
H9-C9-C10	129 (2)	H14-C14-C15	123 (2)
H10-C10-C9	127 (2)	H15-C15-C14	131 (2)
H10-C10-C11	125 (2)	H15-C15-C16	119 (2)
H11-C11-C10	125 (2)	H16-C16-C15	136 (2)
H11-C11-C7	126 (2)	H16-C16-C12	115 (2)

[a] The esd's in parentheses for the interatomic distances and bond angles were calculated from the standard errors of the fractional coordinates of the corresponding atomic positions.

a pair of π-bonding and π^*-antibonding molecular orbitals of the proper symmetry to interact with the available hybridized metal orbitals. A σ bond is formed by donation of an electron pair from the filled π orbital to an empty metal orbital, whereas a π bond is formed by back-donation of an electron pair from a filled metal orbital to the empty π^*-antibonding orbital. Since both removal of electrons from the olefin's π-bonding orbital and donation into its π^*-antibonding orbital weaken the multiple carbon–carbon bond, the corresponding vibrational stretching frequencies are substantially decreased (50–300 cm^{-1}).

For bis(cyclopentadienyl) transition-metal acetylene complexes, a similar qualitative bonding representation can be formulated from a molecular orbital energy level scheme de-

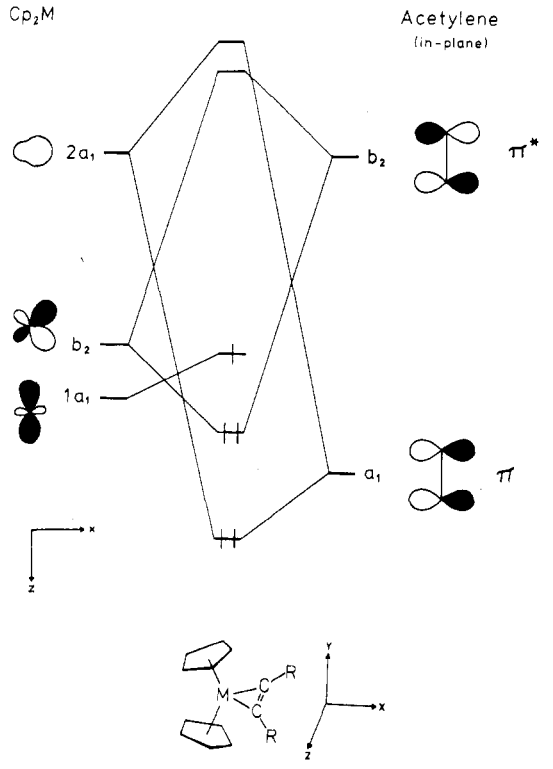

Figure 3. Qualitative molecular energy level scheme for the metal–acetylene interaction in $(\eta^5\text{-}C_5H_5)_2V(C_2R_2)$ complexes.

veloped by Lauher and Hoffmann[33] for the corresponding ethylene complexes, $(\eta^5\text{-}C_5H_5)_2M(C_2H_4)$. Figure 3 depicts the frontier metal orbitals which become available as the angle between the normals to the cyclopentadienyl rings decreases from 180° in the parent metallocene to 135° in the canted derivatives. The lowest energy metal orbitals primarily responsible for bonding are the $1a_1$, b_2, and $2a_1$. From the X-ray diffraction analysis of $(\eta^5\text{-}C_5H_5)_2V(C_2(CO_2CH_3)_2)$, the acetylene bonding interaction occurs primarily within the VC_2 plane which bisects the $(\eta^5\text{-}C_5H_5)_2V$ moiety. Consequently, the out-of-plane π and π^* sets of acetylene orbitals contribute negligibly to the interaction. The remaining filled in-plane π orbital of the acetylene can act as a donor orbital by interaction with the metal $2a_1$ orbital. Two additional electrons are back-donated from the filled metal b_2 to the empty in-plane π^* orbital. These interactions serve to reduce the bond order of the multiple carbon–carbon bond (in accord with the structural results) and also to stabilize the metal b_2 orbital so that it drops below the nonbonding metal a_1 orbital which contains the unpaired electron. Alternatively, this back-bonding interaction can in effect be viewed as oxidizing the metal from V(II) in vanadocene to V(IV) in these $(\eta^5\text{-}C_5H_5)_2V(C_2R_2)$ complexes with the acetylene functioning as a bidentate dicarbanion which coordinates via two σ-type bonds to the vanadium. This description is reasonable in light of the similarities between the structural and magnetic properties observed for the $(\eta^5\text{-}C_5H_5)_2V(C_2R_2)$ and $(\eta^5\text{-}C_5H_5)_2VL_2$ complexes.

Discussion of the EPR Results. The solution and frozen-glass EPR measurements have allowed us to obtain quantitative information about the metal orbital character of the unpaired electron. The solution EPR spectra for the vanadocene adducts resemble closely the spectra obtained for d^1 $(\eta^5\text{-}C_5H_5)_2VL_2$ complexes (L = Cl^-, SCN^-, OCN^-, $SeCN^-$, N_3^-, or $SC_6H_5^-$, or $L_2 = S_5^{2-}$)[34-36] in which the unpaired

(33) Lauher, J. L.; Hoffmann, R. *J. Am. Chem. Soc.* **1976**, *98*, 1729.

Table III. Summary of Results from the Analysis of the Frozen-Glass EPR Data[a]

compd	T_x[b]	T_y	T_z	a	b	a^2/b^2
$(\eta^5\text{-}C_5H_5)_2V(C_2(CO_2CH_3)_2)$	−58.5 (−58.9)	−77.0 (−77.0)	−2.0 (−1.5)	−0.995	0.100	99:1
$(\eta^5\text{-}C_5H_5)_2V(C_2(CF_3)_2)$	−62.5 (−63.0)	−77.5 (−77.6)	−2.0 (−1.4)	−0.997	0.077	168:1
$(\eta^5\text{-}C_5H_5)_2V(N_2(C_6H_5)_2)$	−65.5 (−65.4)	−77.5 (−77.5)	−2.0 (−2.1)	−0.998	0.063	250:1

[a] The values in parentheses are the calculated hyperfine components obtained for the "best" values of a and b. [b] Hyperfine components are given in units of gauss.

electron resides primarily in an a_1 metal orbital. The smaller values of A_{iso} for the vanadocene derivatives (43–46 G) compared to those for the $(\eta^5\text{-}C_5H_5)_2VL_2$-type complexes (60–75 G) reflect a greater degree of electron delocalization in the former systems. The narrow range of the isotropic hyperfine coupling constants observed for the various acetylene, azobenzene, and octafluoro-2-butene adducts indicate that these unsaturated organic molecules are bonded similarly to vanadocene. This remark is supported by the structural determination of the diethyl fumarate derivative by Floriani and co-workers.[9] This vanadacyclopropane adduct is characterized by a trans configuration for the coordinated olefin and is accompanied by an appropriate lengthening of the carbon–carbon double bond to 1.47 (1) Å.

For paramagnetic transition-metal complexes with less than a half-filled d subshell, spin–orbit coupling reduces g_{iso} below the free-electron value of 2.0023. Consequently, an increase in the electron delocalization about the metal is accompanied by a decrease in A_{iso} and an increase in g_{iso} due to the resultant decrease in the spin–orbit contribution. The larger g_{iso} values for the vanadocene derivatives compared to those for the $(\eta^5\text{-}C_5H_5)_2VL_2$ complexes are therefore consistent with the correspondingly smaller A_{iso} values.

Computer simulation of the frozen-glass EPR spectra of several vanadocene adducts has provided an opportunity to estimate the magnitude of the principal components of the **g** and **T** tensors. Although the principal directions of the magnetic tensors with respect to the molecular structure cannot be determined directly for a nonaxial system from the frozen-glass EPR data, the similar solution EPR spectra and overall C_{2v}-$mm2$ symmetry associated with the $(\eta^5\text{-}C_5H_5)_2V(C_2R_2)$ and $(\eta^5\text{-}C_5H_5)_2VL_2$ complexes suggest that the spatial distribution of the unpaired electron in these systems is comparable. Dilute single-crystal EPR studies performed on $(\eta^5\text{-}C_5H_5)_2ML_2$ complexes (M = V,[37] Nb[38]) have shown that the smallest hyperfine component (designated as T_z) is directed normal to the plane which bisects the L–M–L bond angle. For comparison purposes the same coordinate system as defined in Figure 3 (with T_x directed toward the unsaturated molecule and T_y perpendicular to the metallacyclic plane) was used to interpret the frozen-glass EPR data.

The relative metal orbital character within the HOMO can be extracted from a ligand field based analysis of the principal components of the ^{51}V hyperfine tensor.[37] The anisotropic nature of the hyperfine coupling interaction indicates that the electronic ground state consists of an admixture of two or more d orbitals. Under C_{2v}-$mm2$ symmetry the a_1 irreducible representation is the only one which satisfies this requirement.

The ligand field approach generally assumes that the **g** and **T** tensors are coincident and the unpaired electron is localized completely on the vanadium atom. Although this latter condition is not rigorously obeyed, the relative contributions of the two metal orbitals in the electronic ground state represented approximately by

$$|\Psi_0\rangle = a|d_{z^2}\rangle + b|d_{x^2-y^2}\rangle$$

where a and b are mixing coefficients, can be determined. From the application of second-order perturbation theory, suitable relationships for the principal values of the **g** and **T** tensors have been derived in terms of these mixing coefficients.[39] A unique set of coefficients were calculated in each case to provide satisfactory agreement between the observed and calculated hyperfine components. The results, which are summarized in Table III, indicate that the observed anisotropy for the hyperfine interaction arises from the admixture of $3d_{z^2}$ and a small amount of $3d_{x^2-y^2}$ character in the HOMO.

In terms of the assumed coordinate system, the hybridized metal orbital is directed normal to the plane which bisects the VC_2 bond angle. The relative contributions of the two metal AO's can be estimated from the ratio of mixing coefficients a^2/b^2 which for the dimethyldicarboxyacetylene derivative is $-0.995^2/0.100^2 = 99/1$. A comparison of the corresponding values for this ratio with that determined for $(\eta^5\text{-}C_5H_4CH_3)_2VCl_2$[37c] of 20/1 indicates a significantly smaller contribution from the $d_{x^2-y^2}$ AO in the acetylene and azobenzene adducts. This result can be understood by consideration of the difference in magnitude between the L–V–L bond angles for $(\eta^5\text{-}C_5H_4CH_3)_2VCl_2$[37c] and in $(\eta^5\text{-}C_5H_5)_2V(C_2(CO_2CH_3)_2)$ of 87.09 (9) and 35.58 (8)°, respectively. For the dichloride complex electron–electron repulsions prevent the Cl–V–Cl bond angle from closing appreciably, whereas for the acetylene derivative a more acute angle is required since the carbon atoms are directly bonded. From this data it becomes apparent that, as the L–V–L angle decreases, the spatial distribution of the unpaired electron is redistributed to alleviate the accompanying increase in electron repulsion. Since the HOMO consists of an admixture of d_{z^2} and $d_{x^2-y^2}$ AO's, the relative metal character is altered by shifting the electron density from the $d_{x^2-y^2}$ AO to the d_{z^2} orbital (which is directed away from the metal–acetylene interaction). As the $d_{x^2-y^2}$ contribution decreases, the corresponding hyperfine components T_x and T_y become closer in magnitude and a^2/b^2 increases. These EPR studies are not only in accord with the outcome of approximate MO calculations on $(\eta^5\text{-}C_5H_5)_2MoH_2$[40] but provide the *first* quantitative experimental evidence which demonstrates the relationship between the L–M–L bond angle and the metal orbital character of the HOMO in d^1 and d^2 $(\eta^5\text{-}C_5H_5)_2ML_2$-type systems.

Since the magnitude of the C–V–C bond angle in the acetylene (or olefin) adducts is dictated by the V–C and C–C bond distances, one might expect that substituents on the organic substrate could alter these structural and magnetic parameters. Examination of the EPR data in Table III reveals that T_x and the a^2/b^2 ratio appear to be sensitive to variations associated with the coordinated organic substrate. However, in light of the limited amount of available structural and EPR

(34) Doyle, G.; Tobias, R. S. *Inorg. Chem.* **1968**, *7*, 2479.
(35) Muller, E. G.; Watkins, S. F.; Dahl, L. F. *J. Organomet. Chem.* **1976**, *111*, 73.
(36) Muller, E. G.; Petersen, J. L.; Dahl, L. F. *J. Organomet. Chem.* **1976**, *111*, 91.
(37) (a) Petersen, J. L.; Dahl, L. F. *J. Am. Chem. Soc.* **1974**, *96*, 2248. (b) Petersen, J. L.; Dahl, L. F. *Ibid.* **1975**, *97*, 6416. (c) Petersen, J. L.; Dahl, L. F. *Ibid.* **1975**, *97*, 6422.
(38) Petersen, J. L.; Egan, J. W., Jr., manuscript in preparation.
(39) McGarvey, B. R. "Electron Spin Resonance of Metal Complexes"; Yen, T. F., Ed.; Plenum: New York, 1969 (from the Symposium on ESR on Metal Chelates at the Pittsburgh Conference on Analytical Chemistry and Applied Spectroscopy, Cleveland, OH, March 1968).
(40) Petersen, J. L; Lichtenberger, D. L.; Fenske, R. F.; Dahl, L. F. *J. Am. Chem. Soc.* **1975**, *97*, 6433.

data, further studies of a wider range of acetylene, olefin, and diazene derivatives are needed to extend our fundamental understanding of the factors which influence the electronic and molecular structure of this important class of small ring metallacyclic complexes.

Acknowledgment is made to the donors of the Petroleum Research Fund, administered by the American Chemical Society, for support of this work. Computer time for the X-ray diffraction data analysis was provided by the West Virginia Network for Educational Telecomputing.

Registry No. $(\eta^5\text{-}C_5H_5)_2V(C_2(CO_2CH_3)_2)$, 12155-24-7; $(\eta^5\text{-}C_5H_5)_2V(C_2(CF_3)_2)$, 12154-93-7; $(\eta^5\text{-}C_5H_5)_2V(N_2(C_6H_5)_2)$, 51159-66-1; $(\eta^5\text{-}C_5H_5)_2V(C_2(C_6H_5)H)$, 73347-66-7; $(\eta^5\text{-}C_5H_5)_2V(C_2(C_6H_5)_2)$, 73347-67-8; $(\eta^5\text{-}C_5H_5)_2V(FC{=}CF(CF_3)_2)$, 73347-68-9; $(\eta^5\text{-}C_5H_5)_2V$, 1277-47-0.

Supplementary Material Available: Listings of least-squares planes and calculated and observed structure factors (13 pages). Ordering information is given on any current masthead page.

Contribution from the School of Chemical Sciences and Materials Research Laboratory, University of Illinois at Urbana-Champaign, Urbana, Illinois 61801, the Department of Physics, University of Illinois at Urbana-Champaign, Urbana, Illinois 61801, and the Solid State Science Division, Argonne National Laboratory, Argonne, Illinois 60439

Oxidation States of Europium in Zeolites

S. L. SUIB,[1a] R. P. ZERGER,[1a] G. D. STUCKY,*[1a,b] R. M. EMBERSON,[1c] P. G. DEBRUNNER,*[1c] and L. E. ITON*[1d]

Received December 6, 1979

Rare-earth metal ions have proven to be particularly useful in zeolite catalysis, both as stabilizing ions and by virtue of their redox chemistry. In the research reported here, the europium Mössbauer spectra of hydrated and dehydrated europium-exchanged zeolites A, Y, and ZSM-5 have been studied. $Eu(OH)_2{\cdot}H_2O$, used to ion exchange Eu^{2+} into the zeolites, immediately oxidizes to an Eu^{3+} complex in a deoxygenated aqueous solution. This same reaction occurs in the solid state for $Eu(OH)_2{\cdot}H_2O$. An investigation into the role of europium in the thermolytic decomposition of water has been made, and the redox changes from the 3+ to the 2+ oxidation states of europium in zeolites Y and ZSM-5 have been confirmed by EPR. The Mössbauer isomer shifts are sufficiently sensitive to detect the difference in the chemical environment of Eu^{3+} as a consequence of oxidation by chlorine and oxygen. No evidence of Eu^{4+} has been found in an isomer shift range of ±35 mm/s. Metal ions produced by dissolving europium metal in liquid ammonia can be exchanged into the zeolites to give an Eu^{2+} species as indicated by Mössbauer spectroscopy.

Introduction

Europium-exchanged zeolites are of interest because the rare-earth-exchanged zeolites are important as catalysts and because the crystallinity of the zeolites provides cation sites of a definite symmetry. A number of experiments have been performed in order to identify the structural and chemical properties of europium-exchanged zeolites. The presence of Eu^{4+} in zeolite A has been postulated on the basis of X-ray crystallographic evidence.[2,3] Electron paramagnetic resonance has been applied to study the cation locations and ligand coordinations of europium-exchanged mordenite and Y zeolite.[4] A process has been reported for thermolytically dissociating water by using europium-exchanged zeolites.[5] It is believed that europium changes back and forth between the 2+ and 3+ oxidation states in this thermolytic cycle. A Mössbauer study of europium-exchanged mordenite and Y zeolite has been previously reported.[6] In this study these materials were treated with flowing hydrogen at 450 °C which led to nearly complete reduction of Eu^{3+} to Eu^{2+}.

We present here the results of europium Mössbauer measurements on europium-exchanged zeolites A, Y, and ZSM-5 for calcined and hydrated samples. In addition, we show that the $Eu(OH)_2{\cdot}H_2O$ compound is kinetically unstable. The postulated mechanism for the thermochemical decomposition of water catalyzed by europium-exchanged zeolites and the existence of europium(IV) are discussed. Finally, a new method for introducing europium(II) into zeolites is reported.

Experimental Methods

Preparation of Compounds. A. $Eu(OH)_2{\cdot}H_2O$. The compound $Eu(OH)_2{\cdot}H_2O$ was prepared according to the method of Bärnighausen.[7] The lemon yellow material precipitated from a mixture of 0.5 g of europium metal and 20 mL of 10 N NaOH. The reaction was carried out under a pure argon atmosphere by using Schlenkware. All water was distilled, deionized, and deoxygenated. The $Eu(OH)_2{\cdot}H_2O$ was washed with deoxygenated ethanol, dried under vacuum, and subsequently stored in the dark in an argon-filled Vacuum Atmospheres drybox. All starting materials were purchased from Alfa Ventron Co.

B. Europium-Exchanged Zeolite A. In a Schlenk tube 4.5 g of NaA zeolite having a composition of $Na_{12}Al_{12}Si_{12}O_{48}{\cdot}27H_2O$ was added to 200 mL of a saturated aqueous solution of $Eu(OH)_2{\cdot}H_2O$. All solvents mentioned in this report had been distilled and deoxygenated. This reaction was carried out in the dark under an argon atmosphere while the mixture was stirred over a period of 6 days. The resulting zeolite was filtered through a medium frit in the middle of the Schlenk apparatus, the solvent was removed, and the product was then brought into the drybox and stored in the dark in a capped vial. During this procedure the europium-exchanged zeolite was not exposed to oxygen, the atmosphere, or light. Neutron-activation analysis showed that the hydrated A zeolite was 21.5% europium, corresponding to the approximate composition $Eu^{3+}_{3.5}Na_{1.5}Al_{12}Si_{12}O_{48}{\cdot}27H_2O$.

C. Europium-Exchanged Zeolite Y. Approximately 2.0 g of zeolite NaY having a composition $Na_{56}Al_{56}Si_{136}O_{384}{\cdot}256H_2O$ was added to 200 mL of a 0.1 N $EuCl_3{\cdot}6H_2O$ aqueous solution and exchanged while the mixture was stirred for 12 h in a round-bottomed flask. The resulting europium-exchanged zeolite was filtered through a medium frit and stored in a capped vial. Neutron-activation analysis showed that the hydrated Y zeolite was 14.8% europium, corresponding to

(1) (a) School of Chemical Sciences, University of Illinois. (b) Address correspondence to G.D.S. at: Division 5152, Sandia Laboratories, Albuquerque, NM 87185. (c) Department of Physics, University of Illinois. (d) Argonne National Laboratory.
(2) R. L. Firor and K. Seff, *J. Am. Chem. Soc.*, **100**, 976 (1978).
(3) R. L. Firor and K. Seff, *J. Am. Chem. Soc.*, **100**, 978 (1978).
(4) L. E. Iton and J. Turkevich, *J. Phys. Chem.*, **81**, 435 (1977).
(5) P. H. Kasai and R. J. Bishop, Jr., U.S. Patent 3 963 830.
(6) E. A. Samuel and W. N. Delgass, *J. Chem. Phys.*, **62**, 1590 (1975).
(7) H. Bärnighausen, *Z. Anorg. Allg. Chem.*, **342**, 233 (1966).

0020-1669/80/1319-1858$01.00/0